Structures 66 (2024) 106859

Contents lists available at ScienceDirect

Structures

journal homepage: www.elsevier.com/locate/structures

# Frame jack-enhanced viscous damping approach for efficient seismic response mitigation of airport control towers

Kai Yang [a], Zhenhua Xu [b], Yijia Ma [b], Minjun Wu [c], Zhipeng Zhao [c,*], Chao Luo [d]

[a] Shanghai Research Institute of Materials Co. Ltd., Shanghai 200437, China
[b] Sixth Engineering Company of CCCC Fourth Harbor Engineering Co. Ltd., Zhuhai, Guangdong 519000, China
[c] Department of Disaster Mitigation for Structures, Tongji University, Shanghai 200092, China
[d] School of Civil Engineering, Shijiazhuang Tiedao University, Shijiazhuang 050043, China

ARTICLE INFO

*Keywords:*
Airport control tower
Viscous damper
Energy dissipation enhancement
Seismic loads
Vibration control

ABSTRACT

In seismic-prone areas, the construction of airport control towers has been widely undertaken to meet the rapidly expanding transportation demand. Within this context, attention is increasingly drawn towards highly efficient upgrading technologies capable of mitigating bending-mode deformation. A novel approach, defined as the frame jack-enhanced viscous damper (FJ-EVD), is proposed to address seismic response mitigation in airport control towers by strategically employing frame jacks to improve viscous damping. The mechanical model and desired deformation amplification properties of FJ-EVDs are elucidated, followed by the construction of a tower-type structure equipped with FJ-EVDs. Nonlinear time history analysis and parametric investigation are performed to explore the vibration mitigation benefits under seismic excitations characterized by various frequency components. Subsequently, utilizing suggested nonlinear parameter sets and acknowledging the distinctive influence of earthquake types, a displacement amplification-oriented design formula is formulated for the FJ-EVD. Furthermore, the optimized FJ-EVDs are implemented in a typical airport control tower subjected to both far-field earthquakes and pulse-like earthquakes for practical design evaluation. Results demonstrate that the proposed FJ-EVD offers a compact and highly efficient damping solution for enhancing the seismic performance of airport control towers, leveraging the displacement amplification advantages to directly mitigate bending deformations. Following the proposed displacement amplification-oriented design methodology, the FJ-EVD exhibits superior effectiveness and robust control performance compared to conventional viscous dampers optimized under the same criterion. Benefitting from the employed frame jack, only a small installation space is required to facilitate the crossing-story installation, thereby tailoring the proper design parameters and effective bending deformation control for the airport control towers.

## 1. Introduction

Airport control towers serve as critical infrastructure in the civil industry, ensuring a safe and highly efficient operation of air traffic [1–3]. In regions prone to seismic activity, the structural integrity of these tower-like structures becomes paramount to withstand potential seismic-induced excitations [4]. With the increasing demand for air transportation, the construction of airport control towers in the mentioned seismic-prone areas [5] are becoming more prevalent [6,7]. Considerable research has been conducted to examine the dynamic characteristics and collapse mechanisms of tower-type structures under seismic-induced loadings [8,9]. Generally, prior investigations have suggested that the susceptibility of high-rise towers to seismic-induced loadings, particularly the seismic resistance of airport control towers, necessitates significant endeavors to implement cutting-edge vibration control technologies [10–12]. This consensus necessitates advanced structural vibration mitigation measures to enhance the seismic resilience [13–15]. Traditional seismic design approaches for structures like airport control towers primarily focus on mitigating lateral forces using techniques such as base isolation [16–18] or viscous damping systems [19–21]. However, these conventional methods often exhibit limitations when applied to tall and slender structures like control towers, particularly in addressing bending-mode deformations induced by seismic events.

* Corresponding author.
*E-mail address:* zhaozhipeng@tongji.edu.cn (Z. Zhao).

https://doi.org/10.1016/j.istruc.2024.106859
Received 12 April 2024; Received in revised form 11 June 2024; Accepted 29 June 2024
Available online 6 July 2024

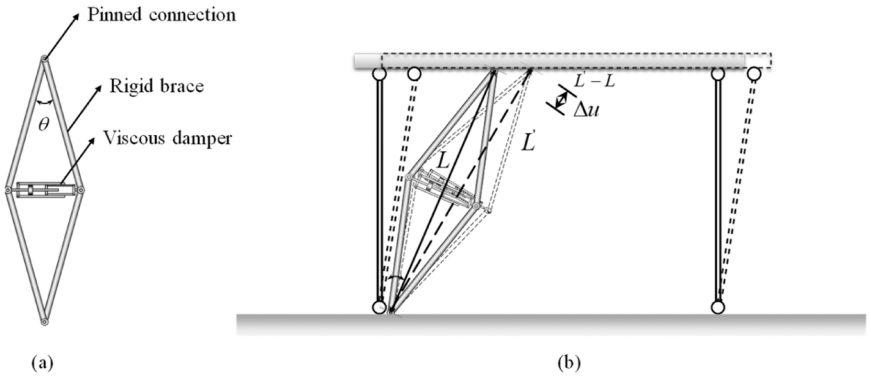


**Fig. 1.** (a) Schematic model of the FJ-EVD and (b) the movement of FJ-EVD.

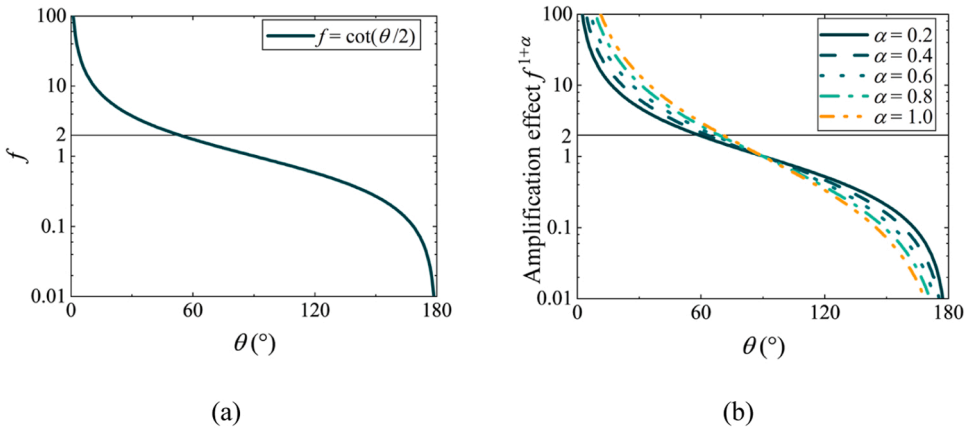


**Fig. 2.** Amplification effect of (a) relative displacement of damper; (b) output damping force of damper.

Conventional viscous dampers have been widely utilized for vibration control in various types of structures and have shown good performance [22–24]. However, for tower-type structures like airport control towers with high lateral stiffness, conventional viscous dampers struggle to achieve maximum damping effect due to the limited shear deformations in the tower-type structure [25]. Addressing this challenge, a novel approach, termed the frame jack-enhanced viscous damper (FJ-EVD) is proposed in this study. Unlike conventional viscous dampers, the FJ-EVD integrates frame jacks strategically to augment the damping capacity, thereby enhancing the seismic performance of the structure. The necessity for such innovative solutions arises from the unique structural characteristics and operational requirements of airport control towers. These structures, characterized by their height and slender profile, are susceptible to significant bending deformations during seismic events, which can jeopardize their functionality and safety [26–30]. Therefore, there is a pressing need to develop effective seismic response control measures tailored to the specific challenges posed by airport control towers. Currently, the majority of research on controlling deformations in tower-type structures during seismic focuses on mitigating lateral deformations, often utilizing technologies like Tuned Mass Dampers [31–34] or Tuned Liquid Dampers [35–38]. However, these approaches fail to adequately address the structural damage posed by bending deformations [39,40], which pose unacceptable risks for critical structures such as airport control towers. This study tackles this challenge by cleverly positioning the FJ-EVD between the floors of the airport control tower. This strategic placement enables the FJ-EVD to convert the tower's bending deformations into damper stroke, effectively controlling seismic responses across a wide range of modal excitations. When subjected to various types of seismic motions, high-rise structures often display unique response patterns [41–44]. The ability to adapt to various seismic excitation scenarios is a crucial factor in assessing the effectiveness of seismic response control devices.

To address these gaps, the FJ-EVD approach is introduced as a pioneering solution to address seismic response challenges encountered in airport control towers. The FJ-EVD method strategically integrates frame jacks to enhance viscous damping effects, thereby bolstering structural resilience. The mechanical model and deformation amplification properties of FJ-EVDs are thoroughly investigated, followed by the fabrication of a tower-type structure integrated with these innovative dampers. Nonlinear time history analysis and comprehensive parametric exploration are employed to scrutinize the efficacy of vibration mitigation across seismic excitations characterized by diverse frequency components. Furthermore, a displacement amplification-oriented design methodology is proposed, taking into account the distinctive influence of earthquake types and optimizing the FJ-EVD parameters to effectively mitigate bending deformations. Subsequently, the recommended nonlinear parameter configurations are leveraged, and the impact of earthquake types is considered in the development of a design formula that emphasizes displacement amplification tailored for FJ-EVDs. The effectiveness of this formula is validated through practical implementation in a standard airport control tower subjected to both far-field earthquakes and pulse-like seismic events, facilitating robust design assessments.

## 2. Frame jack-enhanced viscous damper (FJ-EVD)

To achieve high-level vibration control of an airport control tower subjected to seismic excitation, the FJ-EVD has been introduced due to the constraints of limited installation space. The mechanical configuration and deformation amplification effect of the FJ-EVD are

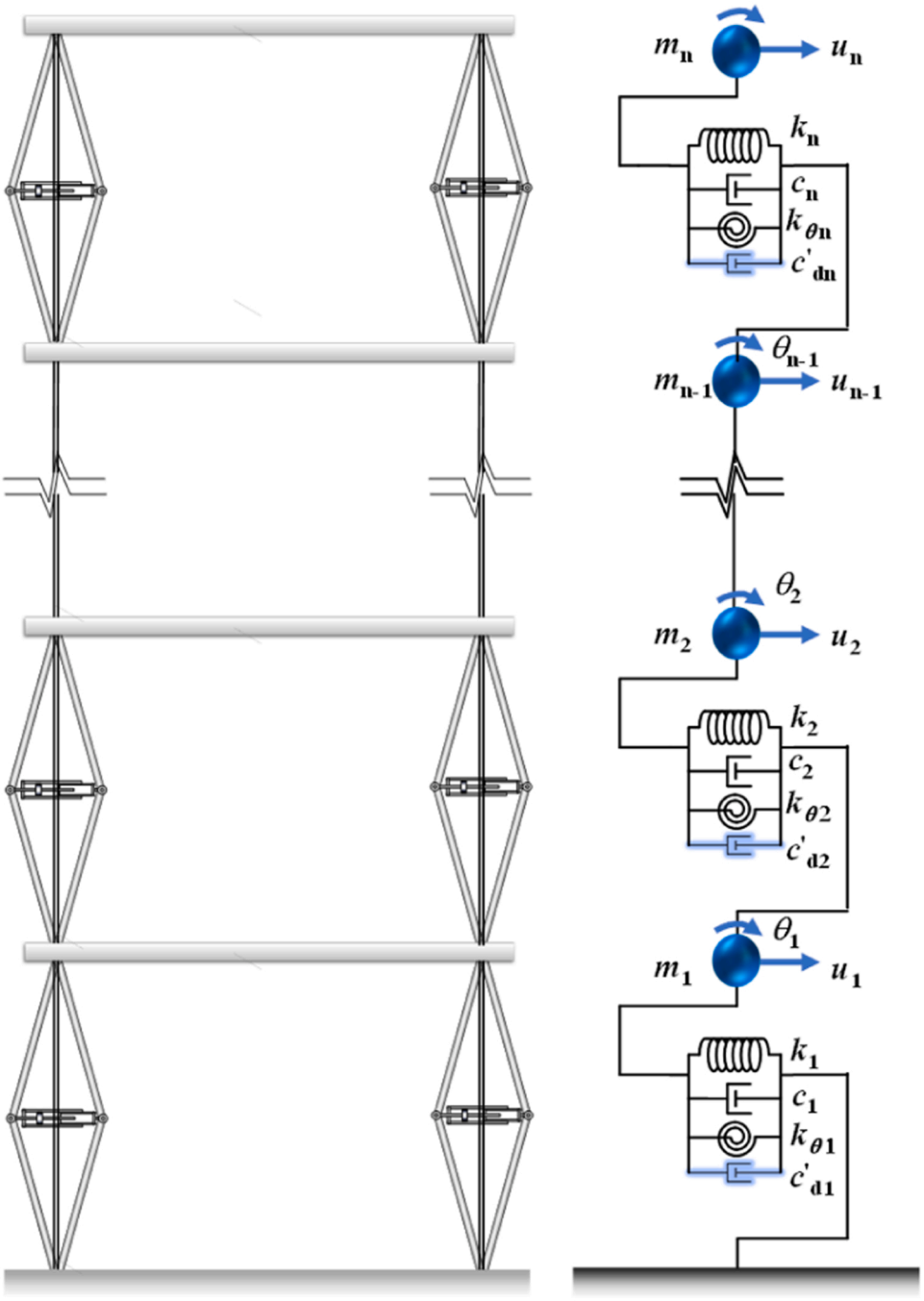


**Fig. 3.** Mechanical model and installation approach fo the FJ-EVDs for the airport control tower structure.

comprehensively explained in a conceptual framework. This framework is integrated with a simplified mechanical model of the controlled FJ-EVD-tower system for the initial analysis. The governing equation corresponding to this model is provided as a reference for subsequent parametric analysis.

### 2.1. Mechanical model and properties

Subjected to seismic excitations, the control tower predominantly undergoes bending deformation, which limits the effectiveness of traditional viscous dampers (VD) due to the relatively small displacement between adjacent floors. Addressing the unique deformation characteristics of the airport control tower, the FJ-EVD has been proposed. This device incorporates a jack-like mechanism and a viscous damper positioned centrally. To achieve the expected deformation amplification, all configurations are connected via hinges. The braces of the frame device are assumed to be rigid, with an angle of $\theta$. This device can be placed between two adjacent floor slabs of the airport control tower structure, connected by hinge joints at either end, as demonstrated in Fig. 1.

### 2.2. Displacement amplification benefit

Through the employment of FJ-EVD, the interlayer displacement of the structure can be amplified, thus permitting dampers in the device to dissipate energy more effectively. As depicted in Fig. 1, the angle between the two braces is $\theta$ and the interlayer displacement is $\Delta u_{\text{Drift}}$. With a small-valued $\Delta u$ triggered by the story movement or rotation, the

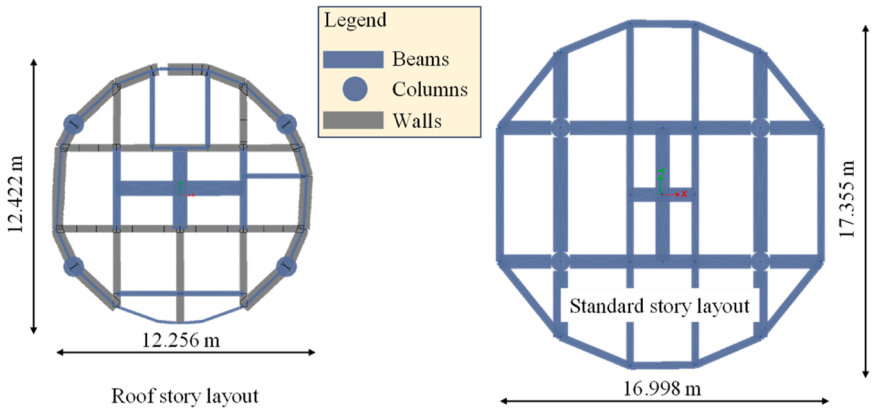


**Fig. 4.** Typical layout of the standard story and the roof within the airport control tower.

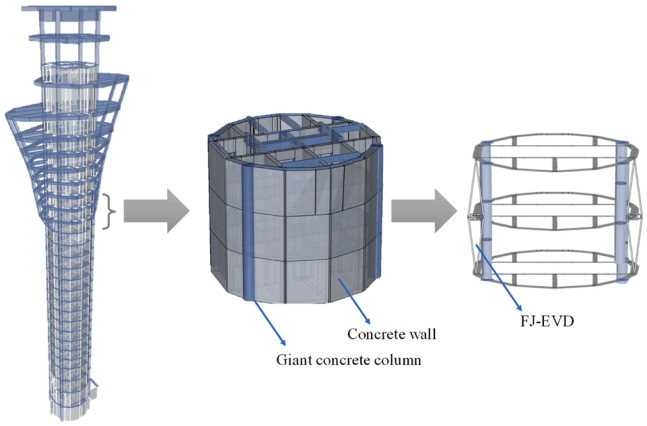


**Fig. 5.** Installation diagram of multiple FJ-EVDs in the airport control tower structure.

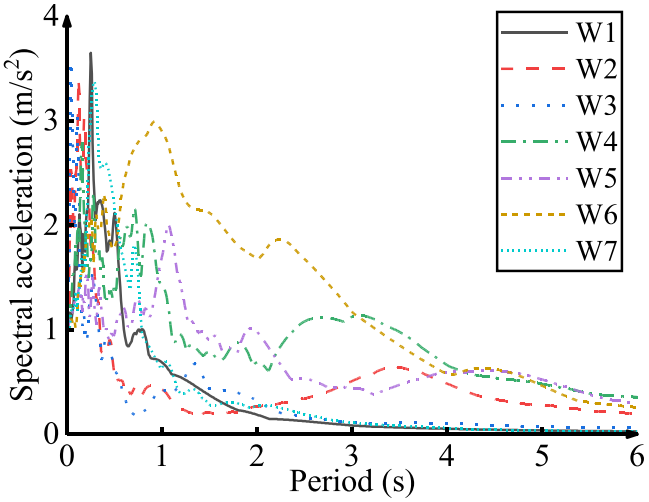


**Fig. 6.** Response spectra of the selected seismic ground motion records for parametric analysis.

**Table 1**
Information of the selected ground motion records for parametric analysis.

| ID | RSN | Year | Event | Magnitude | Station name |
|---|---|---|---|---|---|
| W1 | 125 | 1976 | Friuli_ Italy-01 | 6.50 | Tolmezzo |
| W2 | 174 | 1979 | Imperial Valley-06 | 6.53 | El Centro Array #11 |
| W3 | 767 | 1989 | Loma Prieta | 6.93 | Gilroy Array #3 |
| W4 | 1244 | 1999 | Chi-Chi_ Taiwan | 7.62 | CHY101 |
| W5 | 1503 | 1999 | Chi-Chi_ Taiwan | 7.62 | TCU065 |
| W6 | 2114 | 2002 | Denali_ Alaska | 7.9 | TAPS Pump Station #10 |
| W7 | 753 | 1989 | Loma Prieta | 6.93 | Corralitos |

*Note: RSN denotes the record sequence number in PEER Ground Motion Database [48].

actual deformation of the nonlinear viscous damper can be obtained as:

$$\Delta u_d = \Delta u \cdot f = \Delta u \cdot \cot\frac{\theta}{2} \tag{1}$$

where $\Delta u_d$ is the relative displacement between the two ends of the nonlinear viscous damper, and $f = \cot\frac{\theta}{2}$ is the deformation magnification factor. The nonlinear VD is a velocity-dependent energy dissipation device, of which the output damping force $F_d$ can be determined with respect to the damping exponent $\alpha$ as follows:

$$F_d = c_d|\dot{v}_d|^{\alpha}\mathrm{sgn}(\dot{v}_d) = c_d \cdot f^{\alpha}|\dot{v}|^{\alpha}\mathrm{sgn}(\dot{v}_d) \tag{2}$$

where $c_d$ is the damping coefficient, and $\dot{v}_d$ is the relative velocity between the two ends of the nonlinear viscous damper. Correspondingly, the output force $F_d$ can be amplified by the jack-like device, given which the final force exerted on the airport control tower structure $F$ can be obtained as

$$F = f \cdot F_d = f^{1+\alpha} \cdot c_d|\dot{v}|^{\alpha}\mathrm{sgn}(\dot{v}_d) = c_d'|\dot{v}|^{\alpha}\mathrm{sgn}(\dot{v}_d) \tag{3}$$

where $c_d' = f^{1+\alpha} \cdot c_d$ refers to the pertinent amplified damping coefficient. Eq. (3) indicates that the magnification for the damping force is $f^{1+\alpha}$. By observing Eqs. (1) and (3), the amplification effect for $\Delta u_d$ and $F$ depends on the angle $\theta$ and the damping exponent coefficient $\alpha$, which are plotted in Fig. 2. It is evident that the amplification effect can be achieved when the angle is less than 90°. For the same angle $\theta$, a higher damping exponent coefficient $\alpha$ will produce a greater amplification effect.

In consideration of practical application factors such as support deformation and clearance for device connections, it is crucial to ensure an included angle $\theta$ of less than 60°. This facilitates optimal displacement amplification and damping force.

### 2.3. Installation approach in airport control tower

By installing the proposed FJ-EVD at each layer of the idealized simple structure of the airport control tower, the FJ-EVD-equipped structural model is established as shown in Fig. 3. In particular, a linear damped Multi Degrees of Freedom (MDOF) structure is

**Table 2**
Initial design of FJ-EVDs for the considered airport control tower structure.

| Story | Mass/ton | Damper No. | Total mass/ton | Height/mm |
|---|---|---|---|---|
| 1 | 598.88 | / | / | / |
| 2 | 472.21 | 1 | 1281.04 | 6900 |
| 3 | 402.47 | | | |
| 4 | 406.36 | | | |
| 5 | 312.47 | 2 | 937.42 | 4500 |
| 6 | 312.47 | | | |
| 7 | 312.47 | | | |
| 8 | 312.47 | 3 | 937.42 | 4500 |
| 9 | 312.47 | | | |
| 10 | 312.47 | | | |
| 11 | 312.47 | 4 | 937.42 | 4500 |
| 12 | 312.47 | | | |
| 13 | 312.47 | | | |
| 14 | 312.47 | 5 | 936.53 | 4500 |
| 15 | 312.47 | | | |
| 16 | 311.58 | | | |
| 17 | 312.27 | 6 | 1015.60 | 4500 |
| 18 | 347.98 | | | |
| 19 | 355.36 | | | |
| 20 | 366.89 | 7 | 1180.79 | 4500 |
| 21 | 380.82 | | | |
| 22 | 433.08 | | | |
| 23 | 428.11 | 8 | 1687.34 | 5300 |
| 24 | 507.57 | | | |
| 25 | 751.67 | | | |
| 26 | 659.41 | 9 | 921.48 | 4225 |
| 27 | 262.07 | | | |
| 28 | 272.32 | 10 | 715.70 | 4875 |
| 29 | 443.38 | | | |

considered to represent the equivalent airport control tower excited by seismic excitations. Subjected to the seismic excitation $\ddot{u}_g$, the governing motion equation can be established as:

$$\mathbf{M}\ddot{\mathbf{u}} + (\mathbf{C} + \mathbf{C_d})\dot{\mathbf{u}} + \mathbf{K}\mathbf{u} = -\mathbf{M}\mathbf{r}\ddot{u}_g \tag{4}$$

where **M**, **C**, and **K** denote the mass, Rayleigh damping, and stiffness matrix, $\mathbf{C_d}$ denotes the additional damping provided by the equipped FJ-EVDs, **u** denotes the relative displacement vector at each floor. The mentioned matrixes and vectors are explained as:

$$\begin{aligned}\mathbf{M} &= \begin{bmatrix} m_1 & 0 & \cdots & \cdots & 0 \\ 0 & I_1 & & & \\ & & m_2 & & \\ \vdots & & & I_2 & \vdots \\ \vdots & & & & \ddots \\ & & & & m_n \quad 0 \\ 0 & & \cdots & \cdots & 0 \quad I_n \end{bmatrix}, \mathbf{K} \\ &= \begin{bmatrix} k_1+k_2 & 0 & -k_2 & 0 & \cdots & \cdots & 0 \\ 0 & k_{\theta 1} & & -k_{\theta 2} & & & \\ -k_2 & & k_2+k_3 & & & & \\ 0 & -k_{\theta 2} & & k_{\theta 2}+k_{\theta 3} & & & \vdots \\ \vdots & & & & \ddots & & \\ \vdots & & & & & k_n & 0 \\ 0 & & & \cdots & \cdots & 0 & k_{\theta n} \end{bmatrix}, \mathbf{C} \\ &= \alpha_1 \mathbf{M} + \alpha_2 \mathbf{K}\end{aligned} \tag{5}$$

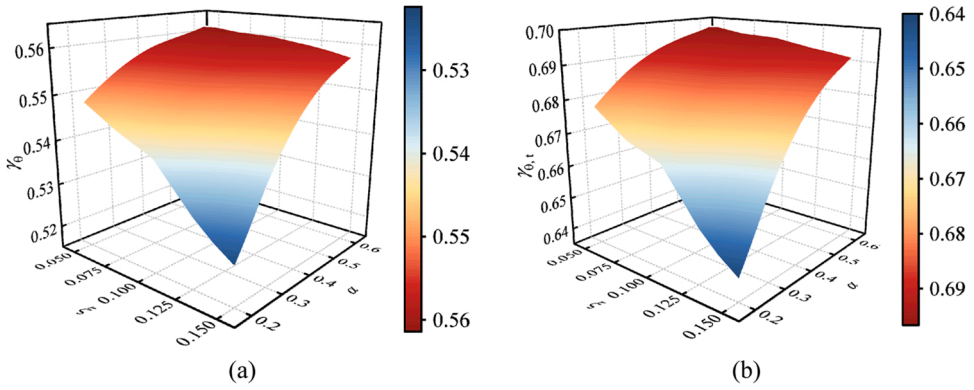


**Fig. 7.** Dynamic response ratios of the airport control tower structure controlled by the FJ-EVDs with the variable damping ratios $\xi \in [0.050, 0.150]$ and damping exponent coefficients $\alpha$: (a) inter-story drift mitigation ratio $\gamma_\theta$ and (b) inter-story drift mitigation ratio of the top story $\gamma_{\theta,t}$.

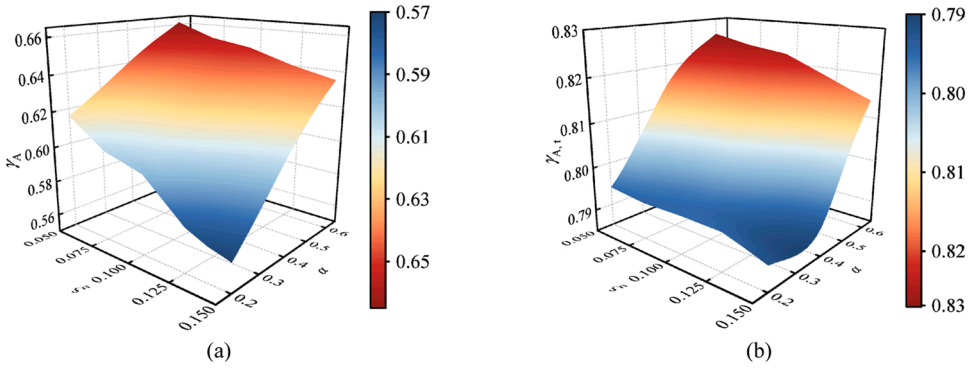


**Fig. 8.** Dynamic response ratios of the airport control tower structure controlled by the FJ-EVDs with the variable damping ratios $\xi \in [0.050, 0.150]$ and damping exponent coefficients $\alpha$: (a) absolute acceleration mitigation ratio $\gamma_A$ and (b) absolute acceleration mitigation ratio of the top story $\gamma_{A,t}$.

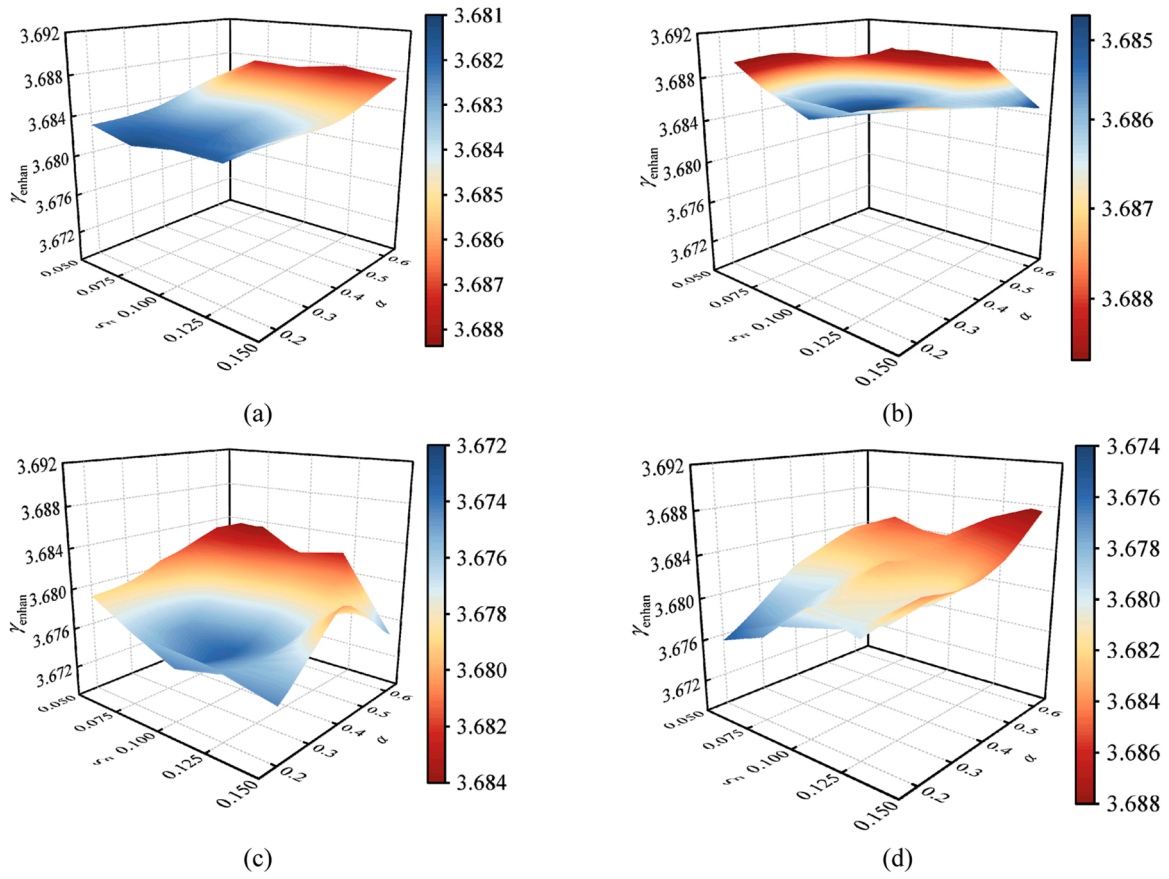


**Fig. 9.** Damping enhancement ratios $\gamma_{enhan}$ of FJ-EVDs attached to the airport control tower structure with the variable damping ratios $\xi \in [0.050, 0.150]$ and damping exponent coefficients $\alpha$: (a) FJ-EVD-1 on the 1st-4th floor, (b) FJ-EVD-2 on the 1st-4th floor, (c) FJ-EVD-1 on the 13th-16th floor, and (d) FJ-EVD-2 on the 13th-16th floor.

$$\mathbf{C_d} = \begin{bmatrix} 0 & 0 & 0 & 0 & \cdots & \cdots & 0 \\ 0 & (c'_{d1} + c'_{d2})l_s & 0 & -c'_{d2}l_s & & & \\ 0 & 0 & 0 & 0 & & & \\ 0 & -c'_{d2}l_s & 0 & (c'_{d2} + c'_{d3})l_s & & & \vdots \\ \vdots & & & & \ddots & & \vdots \\ \vdots & & & & & 0 & 0 \\ 0 & & & \cdots & \cdots & 0 & c'_{dn}l_s \end{bmatrix} \tag{6}$$

$$\mathbf{r} = \{1, 0, 1, 0 \cdots 1, 0\}^T \tag{7}$$

$$\mathbf{u} = \{u_1, \theta_1, u_2, \theta_2, \cdots u_n, \theta_n\}^T \tag{8}$$

where $l_s$ refers to the half-length of the story along the installation direction.

Given the FJ-EVD-equipped tower structure and ground motion records, the time history responses can be numerically solved using the software ETABS [45]. Particularly, the amplified damping coefficient listed in Eq. (6) comprehensively reflects the contribution of the brace angle $\theta$ and nonlinear damping exponent $\alpha$. The displacement amplification benefit forms the enhanced energy dissipation and rotational response control of the FJ-EVD for the airport control tower structure.

## 3. FJ-EVD-based vibration benefits of airport control towers

In this section, the essential seismic vibration control problem for the aircraft control tower is addressed by employing the FJ-EVD, utilizing its verified effectiveness and parameter design methodology. By exploiting the displacement amplification effect and frame-jack installation approach, the FJ-EVD can be effectively utilized in controlling vibrations in airport control towers and other tall, slender structures.

### 3.1. Overview of airport control towers

The architecture of a typical airport control tower is comprised of a cylindrical structure constructed from reinforced concrete material, as depicted in Fig. 4. A total mass of 10,650 tons is possessed, with the first mode having a generalized mass of 2960 tons. The height of the tower, including the platform on the roof, is 96.6 m. Around the perimeter, there are 4 giant concrete circular columns spaced, interconnected by a 500 mm thick concrete shear wall ring with a diameter of 12 m, collectively forming a circular structural layout. The finite element analysis model of this airport control tower is established in the commercial software ETABS [46]. The ultimate strength of the concrete in the tower is 30 MPa and 40 MPa for the cylindrical shell below 52.8 m and above 52.8 m, respectively, whereas the ultimate strength for all floors is 30 MPa. The Rayleigh damping ratio is adopted as 0.05 in the dynamic response analysis [45] for the airport control towers under

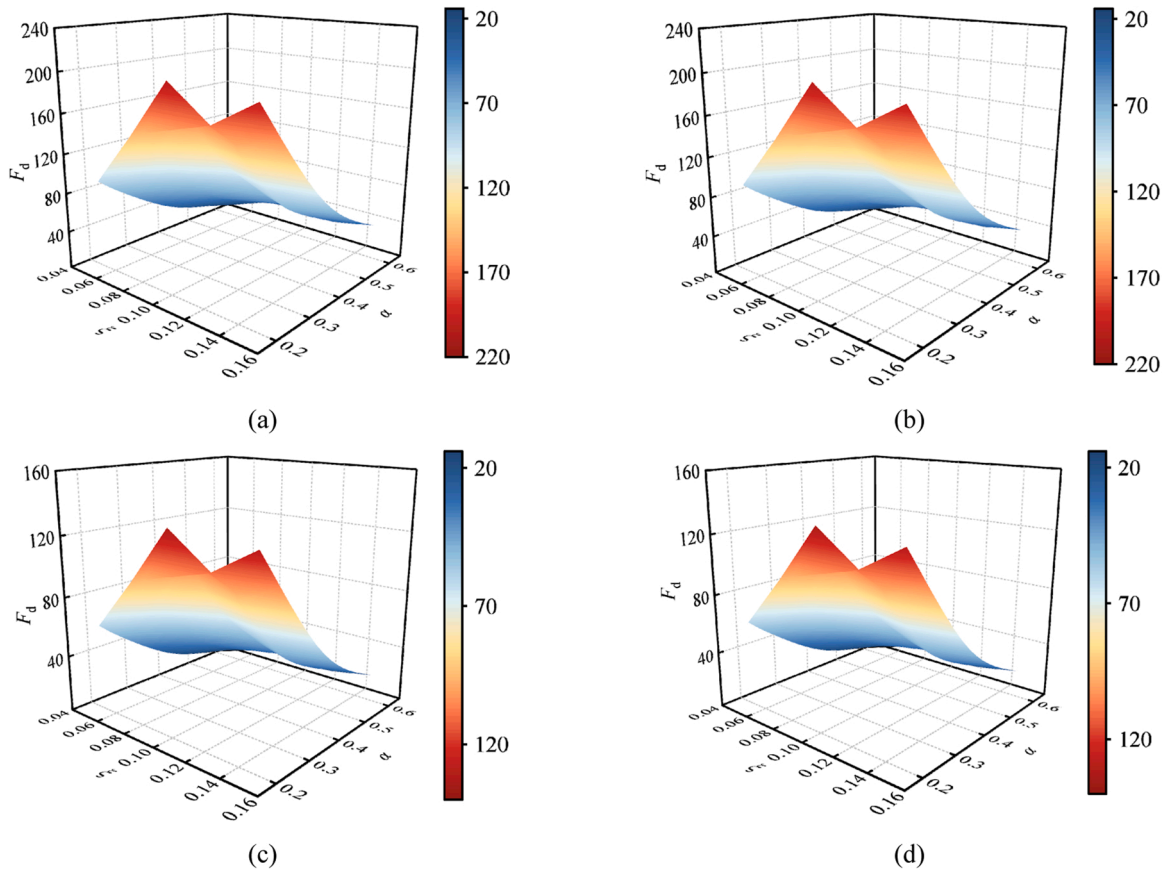


**Fig. 10.** Maximum output force of viscous damper $F_d$ within FJ-EVDs attached to the airport control tower structure with the variable damping ratios $\xi \in [0.050, 0.150]$ and damping exponent coefficients $\alpha$: (a) FJ-EVD-1 on the 1st-4th floor, (b) FJ-EVD-2 on the 1st-4th floor, (c) FJ-EVD-1 on the 13th-16th floor, and (d) FJ-EVD-2 on the 13th-16th floor.

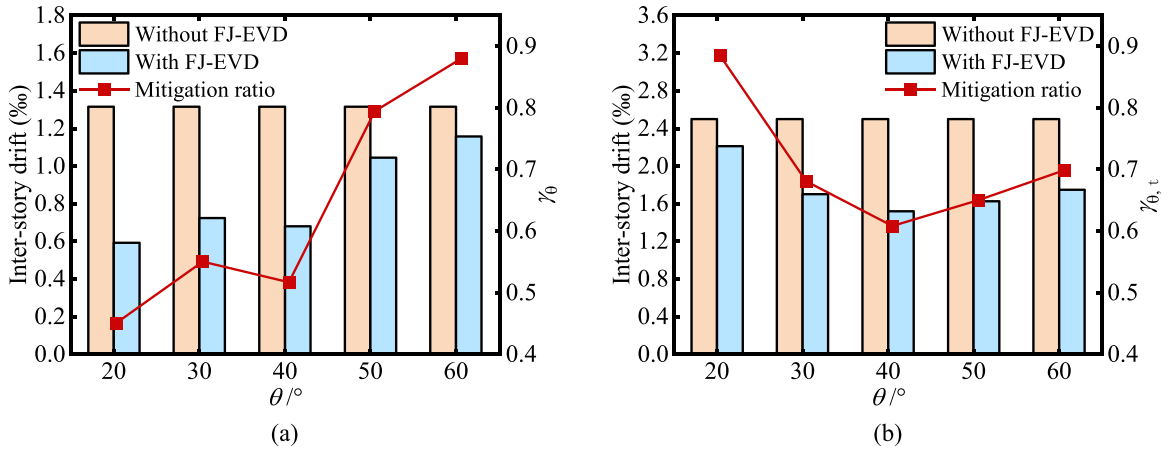


**Fig. 11.** Dynamic response and mitigation ratios of the airport control tower structure controlled by the FJ-EVDs with the variable control angles $\theta$, damping ratio $\xi = 0.075$, and damping exponent coefficient $\alpha = 0.3$: (a) inter-story drift mitigation ratio $\gamma_\theta$ and (b) inter-story drift mitigation ratio of the top story $\gamma_{\theta,t}$.

seismic excitations.

The control tower has a cylindrical configuration, which restricts the internal space due to cylindrical walls and connecting beams. However, FJ-EVD can still be installed in areas without any internal partitions. For a flexible deformation control along the height of the airport control towers, the FJ-EVDs can be set up in multiple layers, as demonstrated in Fig. 5.

### 3.2. Performance evaluation indices

For the multiperformance assessment, a series of performance indicators is defined for the airport control tower under seismic excitation, including the inter-story drift mitigation ratio of the structure and top floor, $\gamma_\theta$ and $\gamma_{\theta,t}$ namely, absolute acceleration mitigation ratio the structure and top floor, $\gamma_A$ and $\gamma_{A,t}$ namely. For the FJ-EVDs, the performance can be evaluated by the damping enhancement ratio $\gamma_{enhen}$. The mentioned performance ratios can be expressed in detail as:

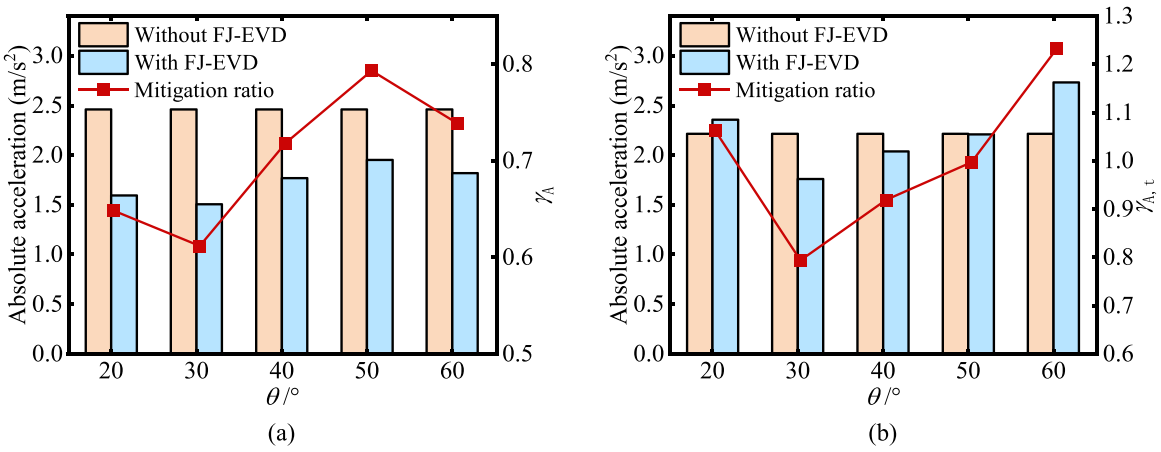


**Fig. 12.** Dynamic response and mitigation ratios of the airport control tower structure controlled by the FJ-EVDs with the variable control angles $\theta$, damping ratio $\xi = 0.075$, and damping exponent coefficient $\alpha = 0.3$: (a) absolute acceleration mitigation ratio $\gamma_A$ and (b) absolute acceleration mitigation ratio of the top story $\gamma_{A,t}$.

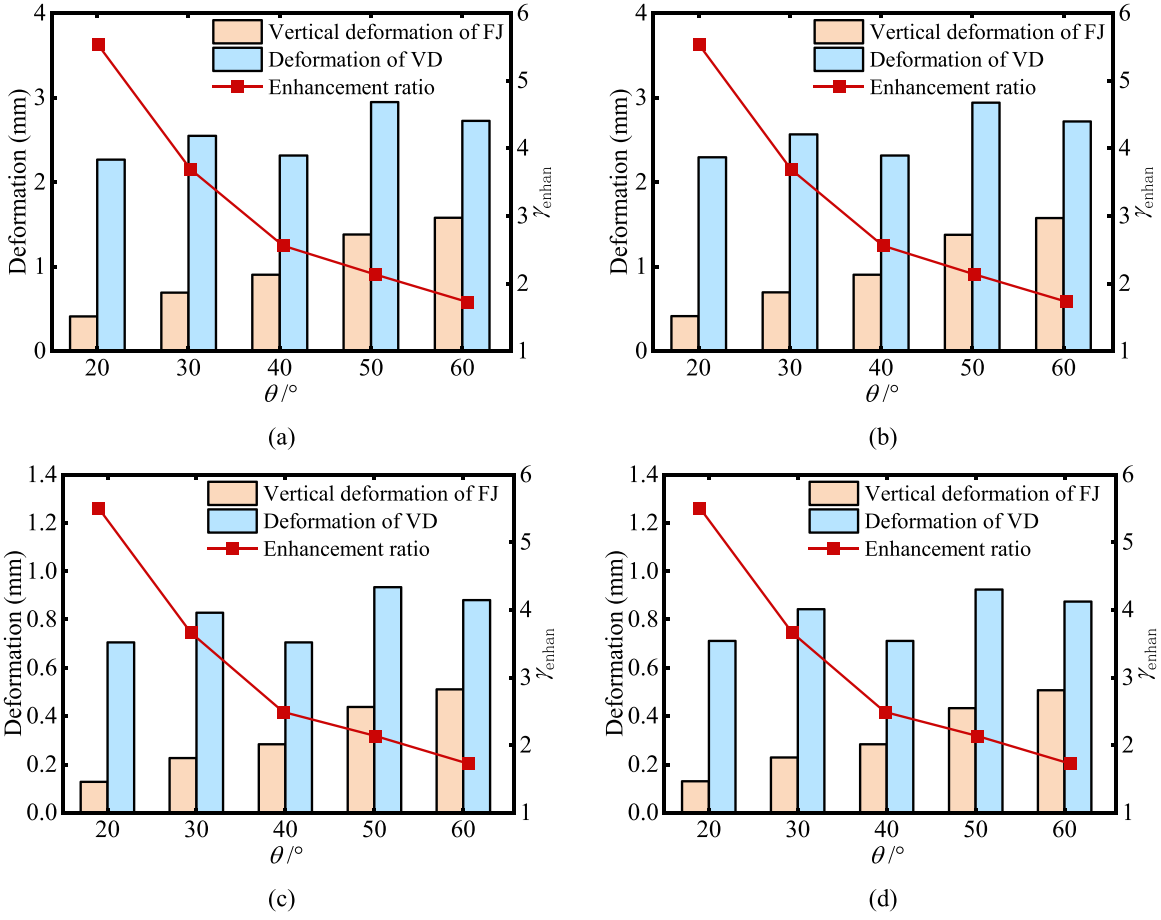


**Fig. 13.** Deformation and damping enhancement ratios $\gamma_{enhan}$ of FJ-EVDs attached to the airport control tower structure with the variable control angles $\theta$, damping ratio $\xi = 0.075$, and damping exponent coefficient $\alpha = 0.3$: (a) FJ-EVD-1 on the 1st-4th floor, (b) FJ-EVD-2 on the 1st-4th floor, (c) FJ-EVD-1 on the 13th-16th floor, and (d) FJ-EVD-2 on the 13th-16th floor.

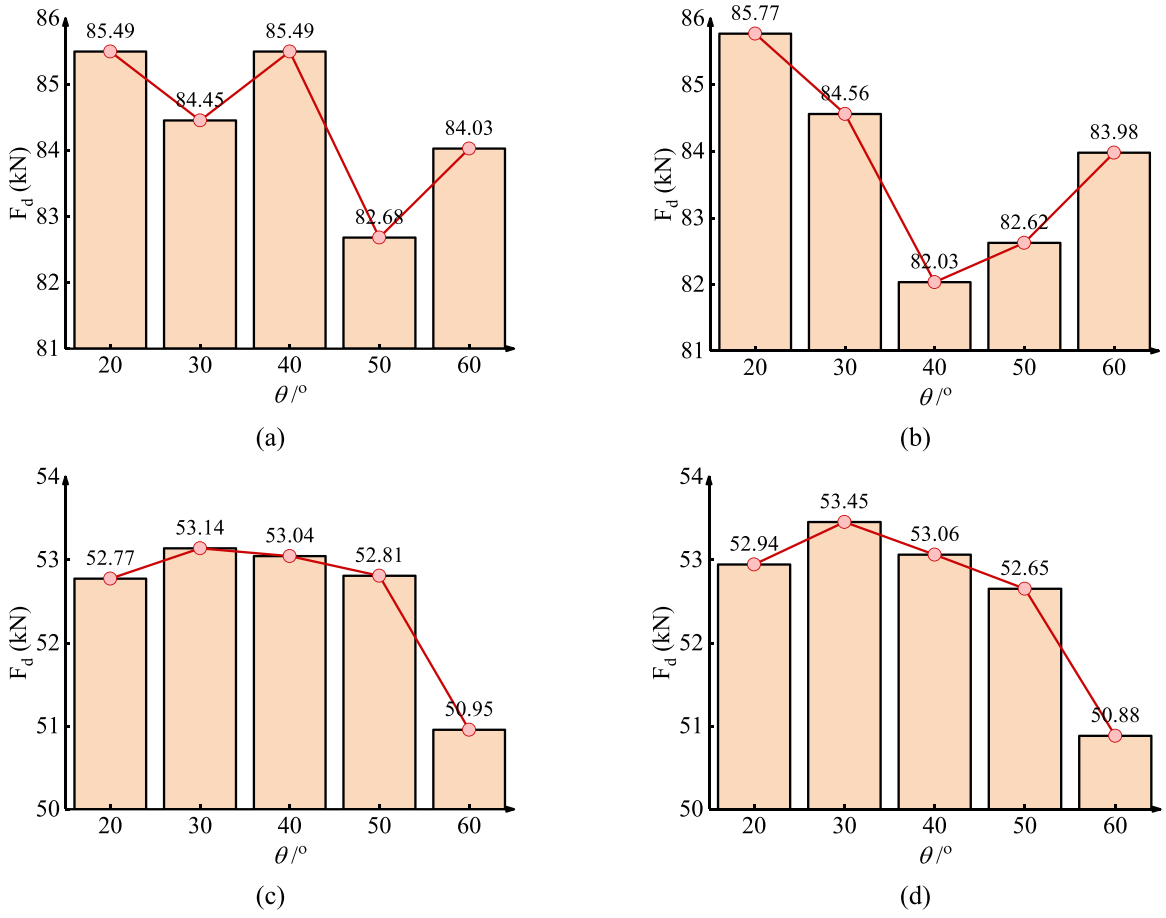


**Fig. 14.** Maximum output force of viscous damper $F_d$ within FJ-EVDs attached to the airport control tower structure with the variable control angles $\theta$, damping ratio $\xi = 0.075$, and damping exponent coefficient $\alpha = 0.3$: (a) FJ-EVD-1 on the 1st-4$^{th}$ floor, (b) FJ-EVD-2 on the 1$^{st}$-4$^{th}$ floor, (c) FJ-EVD-1 on the 13$^{th}$-16$^{th}$ floor, and (d) FJ-EVD-2 on the 13$^{th}$-16$^{th}$ floor.

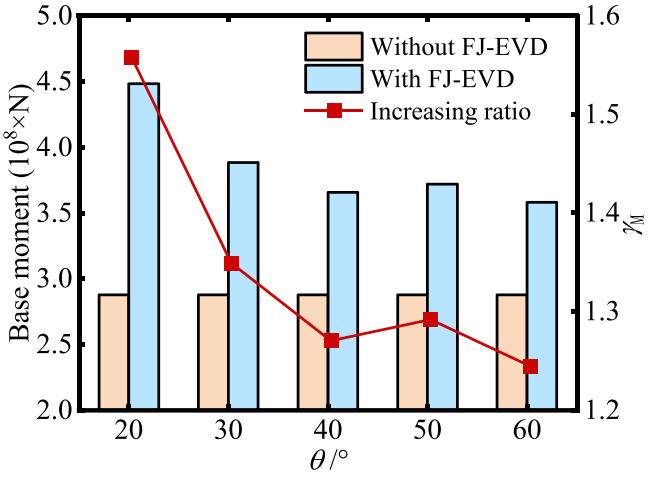


**Fig. 15.** Base moment and increasing ratio $\gamma_M$ of the airport control tower structure controlled by FJ-EVDs with the variable control angles $\theta$, damping ratio $\xi = 0.075$, and damping exponent coefficient $\alpha = 0.3$.

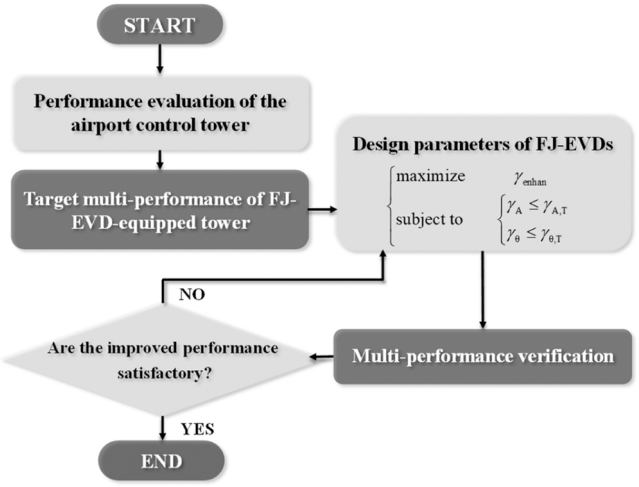


**Fig. 16.** Flowchart of the displacement amplification capacity-based design procedure of the FJ-EVDs for the airport control tower.

**Table 3**
Originality of the selected ground motion records for the case investigation.

| ID | RSN | Type | Year | Event | Magnitude | Station name |
|---|---|---|---|---|---|---|
| W8 | / | Artificial wave | / | / | / | / |
| W9 | 825 | Near-field earthquake | 1992 | Cape Mendocino | 7.01 | Cape Mendocino |
| W10 | 960 | Far-field earthquake | 1994 | Northridge-01 | 6.69 | Canyon Country – W Lost Cany |
| W11 | 828 | Pulse earthquake | 1992 | Cape Mendocino | 7.01 | Petrolia |

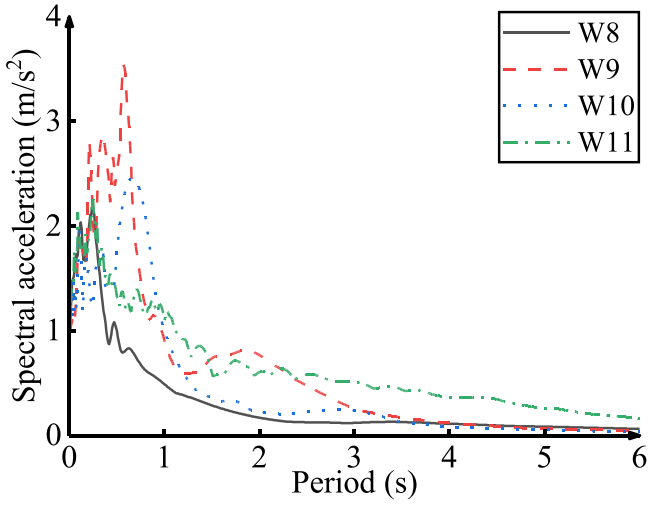


**Fig. 17.** Response spectra of selected ground motion records for the case analysis.

**Table 4**
Optimal parameters of the designed FJ-EVD for airport control tower structures.

| ID | Location | Damping coefficient $c_{d,j}$ | Damping exponent coefficient $\alpha$ | Control angle $\theta$ |
|---|---|---|---|---|
| 1 | $1^{st}$ – $4^{th}$ floor | 60.50 | 0.3 | 30 |
| 2 | $5^{th}$ – $7^{th}$ floor | 44.27 | 0.3 | 30 |
| 3 | $8^{th}$ – $10^{th}$ floor | 44.27 | 0.3 | 30 |
| 4 | $11^{th}$ – $13^{th}$ floor | 44.27 | 0.3 | 30 |
| 5 | $14^{th}$ – $16^{th}$ floor | 44.23 | 0.3 | 30 |
| 6 | $17^{th}$ – $19^{th}$ floor | 47.96 | 0.3 | 30 |
| 7 | $20^{th}$ – $22^{nd}$ floor | 55.76 | 0.3 | 30 |
| 8 | $23^{rd}$ – $25^{th}$ floor | 79.68 | 0.3 | 30 |
| 9 | $26^{th}$ – $27^{th}$ floor | 43.52 | 0.3 | 30 |
| 10 | $27^{th}$ – $29^{th}$ floor | 33.80 | 0.3 | 30 |

$$\text{Forstructure}\begin{cases}\gamma_\theta=\dfrac{\max\left[\left(u_{i,1}-u_{i-1,1}\right)/h_i\right]}{\max\left[\left(u_{i,0}-u_{i-1,0}\right)/h_i\right]},\gamma_{\theta,t}=\dfrac{\max\left[\left(u_{n,1}-u_{n-1,1}\right)/h_n\right]}{\max\left[\left(u_{n,0}-u_{n-1,0}\right)/h_n\right]}\\ \gamma_A=\dfrac{\max\left(\ddot{u}_{i,1}+\ddot{u}_g\right)}{\max\left(\ddot{u}_{i,0}+\ddot{u}_g\right)},\gamma_{A,t}=\dfrac{\max\left(\ddot{u}_{n,1}+\ddot{u}_g\right)}{\max\left(\ddot{u}_{n,0}+\ddot{u}_g\right)}\end{cases}$$
$$\text{ForFJ}-\text{EVDs}\begin{cases}\gamma_{enhan}=\dfrac{\max\left(u_{d,j}\right)}{\max\left(u_{f,j}\right)}\end{cases} \tag{9}$$

where $u_{i,1}$ and $u_{i,0}$ are the displacement of the controlled and uncontrolled structure in the $i^{th}$ floor, $u_{n,1}$ and $u_{n,0}$ represent the displacement of the controlled and uncontrolled structure in the top floor, $n^{th}$ floor namely, $\ddot{u}_{i,1}$ and $\ddot{u}_{i,0}$ denote the relative acceleration of the controlled and uncontrolled structure in the $i^{th}$ floor, $\ddot{u}_{n,1}$ and $\ddot{u}_{n,0}$ are the relative acceleration of the controlled and uncontrolled structure in the top floor, $u_{d,j}$ and $u_{f,j}$ denote the deformation of the VD and vertical deformation of the frame jack in the $j^{th}$ FJ-EVD.

Considering the stochastic nature of earthquakes, the multi-benefit of the tower subjected to long-period seismic ground motions is further examined using four far-field ground motion records (W1-W4) and three near-fault ground motion records (W5-W7) selected from the PEER database. The specific information is summarized in Table 1, of which the acceleration spectra are normalized by the peak ground acceleration and shown in Fig. 6. According to the Chinese Code for seismic design of buildings [47], the peak ground acceleration of the earthquakes is assumed as 0.10 g to execute the nonlinear time history analysis.

### 3.3. Parametric investigation and effectiveness

The installation of FJ-EVDs has been found to improve the deformation characteristics of the VD and enhance its energy dissipation efficiency. Consequently, the seismic performance of the airport control tower is closely related to the design parameters of the FJ-EVD. To address the discrepancy between theoretical analysis and practical application, a parameter analysis is conducted to evaluate the vibration mitigation effect of the FJ-EVDs on structural performances, including the maximum inter-story drift, maximum absolute acceleration, and base moment, as well as the damping enhancement effect of the FJ-EVDs.

Before the execution of the parameter analysis, the original structure is initially analyzed to determine of the design parameters of FJ-EVDs, of which the first structural period $T$ is 2.01 s. The detailed mass information is shown in Table 2. The designed damping coefficient $c_{d,j}$ of the $j^{th}$ FJ-EVD can be defined as:

$$c_{d,j}=2m_j\omega_1\xi=\frac{4\pi m_j\xi}{T} \tag{10}$$

where $\omega_1$ denotes the first circular frequency of the primary structure, $\xi$ represents the nominal damping ratio of the FJ-EVDs, $m_j$ is the total layer mass of the multiple layer that the $j^{th}$ FJ-EVD is installed.

In the analysis procedure, the earthquake waves illustrated in Fig. 6 are employed to carry out time history analysis, during which the peak ground acceleration is set as 1 m/s$^2$. Constraining the control angle $\theta = 30^0$, the nominal damping ratio $\xi$ is varied from 0.05 to 0.15, while the damping exponent coefficient $\alpha$ is changed from 0.2 to 0.6. The corresponding average inter-story drift mitigation ratio and absolute acceleration mitigation ratio of the airport control tower structure can be obtained by repetitive time-domine calculation, of which their relationship with $\xi$ and $\alpha$ are depicted in Fig. 7 and Fig. 8, while the damping enhancement effect of the FJ-EVDs and the maximum output force of the VDs within the FJ-EVDs are illustrated in Fig. 13 and Fig. 14. It can be observed from these figures that the minimum values of both the inter-

**Table 5**
Time history analysis results of the original airport control tower structure (ST0) and controlled airport control tower structures (ST1, ST2).

| Earthquake | Maximum inter-story drift (‰) | | | | | Maximum absolute acceleration (m/s2) | | | | |
|---|---|---|---|---|---|---|---|---|---|---|
| | ST0 | ST1 | $\gamma_0$ | ST2 | $\gamma_0$ | ST0 | ST1 | $\gamma_A$ | ST2 | $\gamma_A$ |
| W8 | 2.50 | 1.67 | 0.67 | 2.45 | 0.98 | 2.46 | 1.75 | 0.71 | 2.22 | 0.90 |
| W9 | 1.65 | 1.02 | 0.62 | 1.62 | 0.99 | 1.97 | 1.46 | 0.74 | 1.92 | 0.97 |
| W10 | 4.36 | 2.69 | 0.62 | 4.31 | 0.99 | 3.49 | 3.18 | 0.91 | 3.43 | 0.98 |
| W11 | 2.05 | 1.43 | 0.70 | 2.02 | 0.99 | 2.32 | 1.72 | 0.74 | 2.28 | 0.99 |
| AVE | 2.64 | 1.70 | 0.65 | 2.60 | 0.98 | 2.56 | 2.03 | 0.79 | 2.46 | 0.97 |

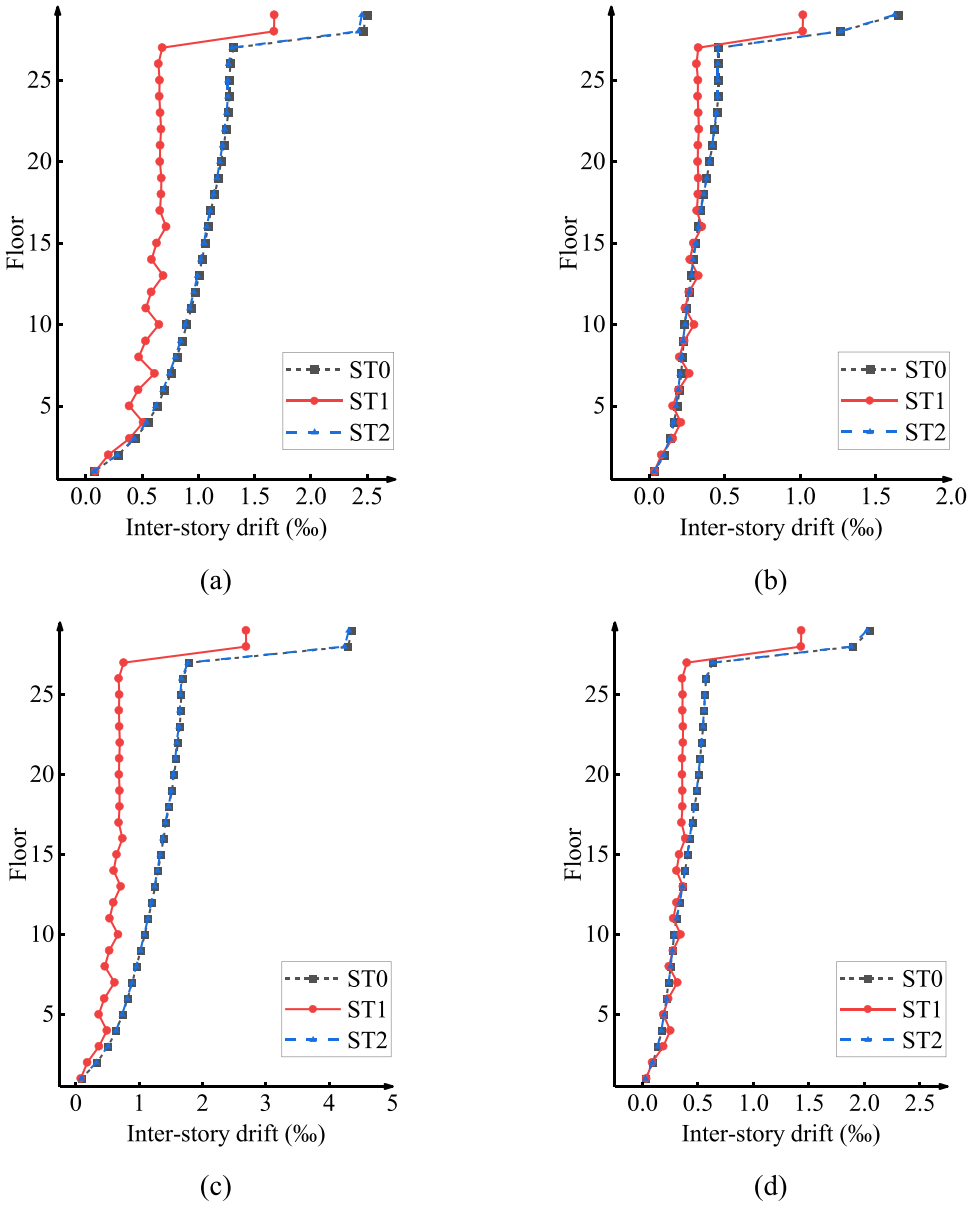


**Fig. 18.** Maximum inter-story drift responses of the ST0, ST1 and ST2 under the (a) artificial wave, (b) near-fault earthquake, (c) far-field earthquake, and (d) pulse earthquake.

story drift mitigation ratio and absolute acceleration mitigation ratio occur when the nominal damping ratio $\xi$ and the damping exponent coefficient $\alpha$ of the FJ-EVDs take the minimum at the same time, and the control effect of the FJ-EVDs on the top floor of the structure is worse than the remained floors. As for the damping enhancement effect, it seems that it is not sensitive to the nominal damping ratio $\xi$ and the damping exponent coefficient $\alpha$ of the FJ-EVDs. The control forces of the VDs within the FJ-EVDs are less when the $\alpha$ are set as larger values..

To explore the influence of the control angle of the FJ-EVD on its seismic mitigation efficiency, the nominal damping ratio $\xi$ and the damping exponent coefficient $\alpha$ are constrained as 0.075 and 0.3, while the control angle $\theta$ is changed from $20^0$ to $60^0$, of which the analysis results are shown in Figs. 11–15. As illustrated in Fig. 11, the control effect of the FJ-EVDs on the inter-story drift of the top floor is observed to initially decrease and then increase as the control angle $\theta$ is increased, while that of the remaining floors demonstrates a primarily increasing

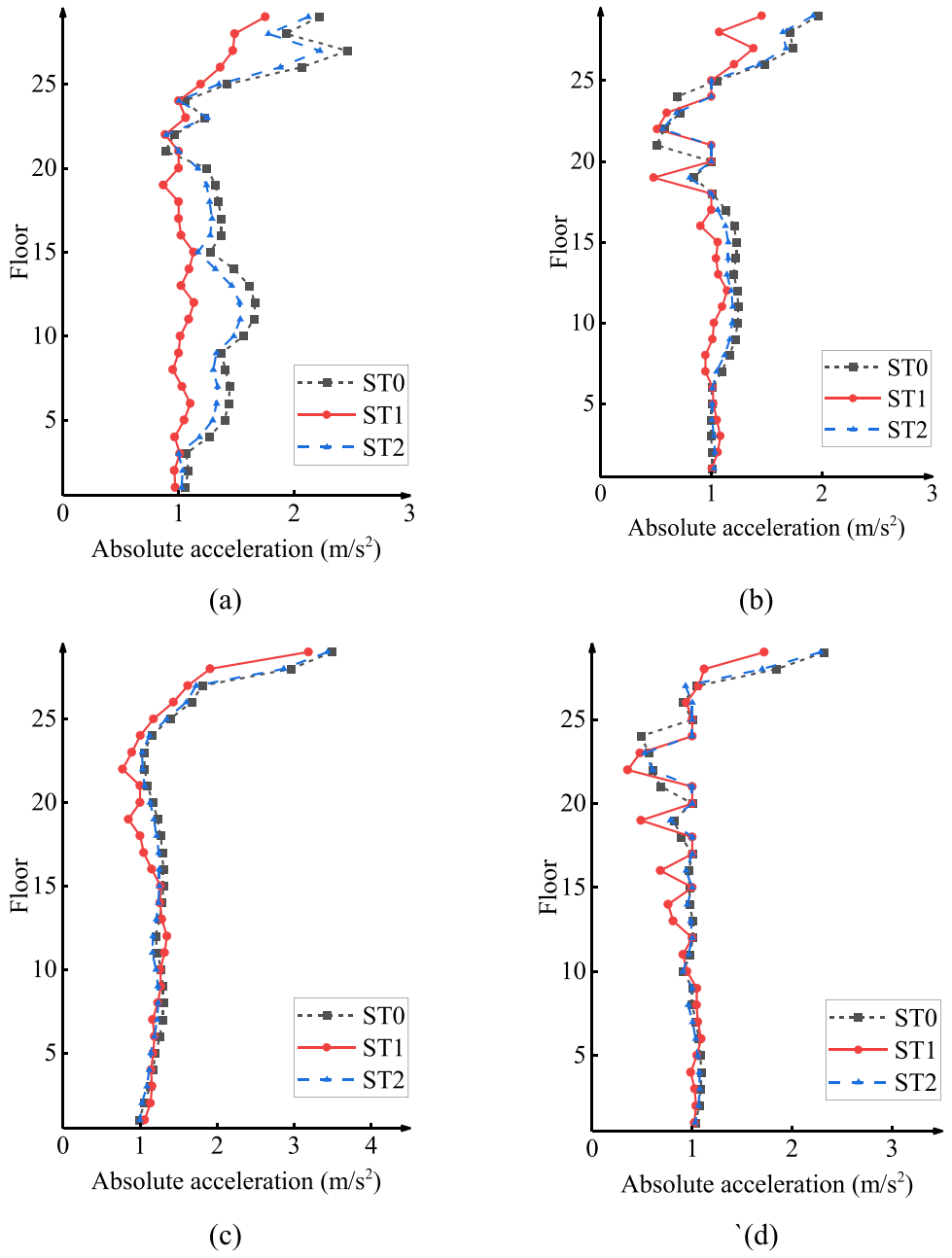


**Fig. 19.** Maximum absolute acceleration responses of the ST0, ST1 and ST2 under the (a) artificial wave, (b) near-fault earthquake, (c) far-field earthquake, and (d) pulse earthquake.

trend. Regarding the absolute acceleration control effect in Fig. 12, both the top floor and remaining floors exhibit a trend of first decreasing and then increasing absolute acceleration mitigation ratios. However, as highlighted in Fig. 13 and Fig. 14, the damping enhancement effect of the FJ-EVD is evidently linked to its control angle, displaying a negative correlation, while the control force exerted by the FJ-EVDs exhibits a roughly negative correlation to the variation trend of change in control angles. In summary, it is evident that simultaneous optimization of the airport control tower structure's performance and the damping enhancement efficiency of FJ-EVD cannot be achieved. Therefore, maintaining a balance between them in the design procedure is of great importance.

### *3.4. Displacement amplification-oriented design of FJ-EVD*

Following the presented parametric analysis results, the multiple FJ-EVDs produce an energy dissipation enhanced approach for the seismic-induced responses mitigation of the airport control tower. With the aid of frame jack mechanism and crossing-floor installation method, the viscous dampers can be triggered by amplified deformations.

Consequently, the vibration mitigation benefits can be realized and beneficial to limit the multiple seismic responses of the airport control tower by using the limited installation space. Given the desirable advantage of the FJ-EVD, a displacement amplification capacity-based design is established in this section. The maximum inter-story drift mitigation ratio $\gamma_\theta$ and maximum absolute acceleration mitigation ratio $\gamma_A$ are set as constraint conditions which needs to meet the requirement for the preset target values, while maximizing the damping enhancement ratio $\gamma_{enhan}$ is set as the optimal target. The proposed demand-oriented design problem can be mathematically expressed as

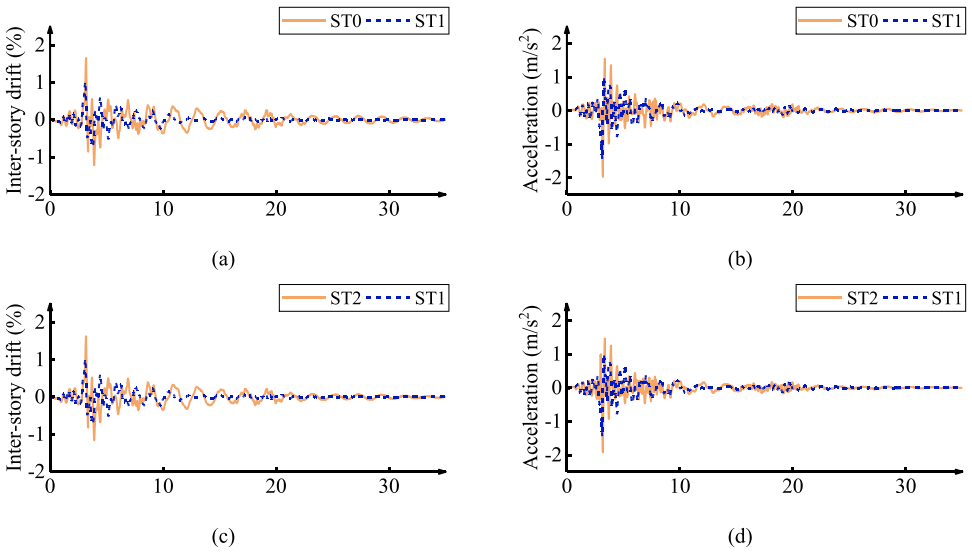


**Fig. 20.** Time history curves of the 29th floor on the ST0, ST1 and ST2 under W9, including the comparison of (a) inter-story drift and (b) absolute acceleration between the ST0 and ST1, as well as the comparison of (c) inter-story drift and (d) absolute acceleration between the ST1 and ST2.

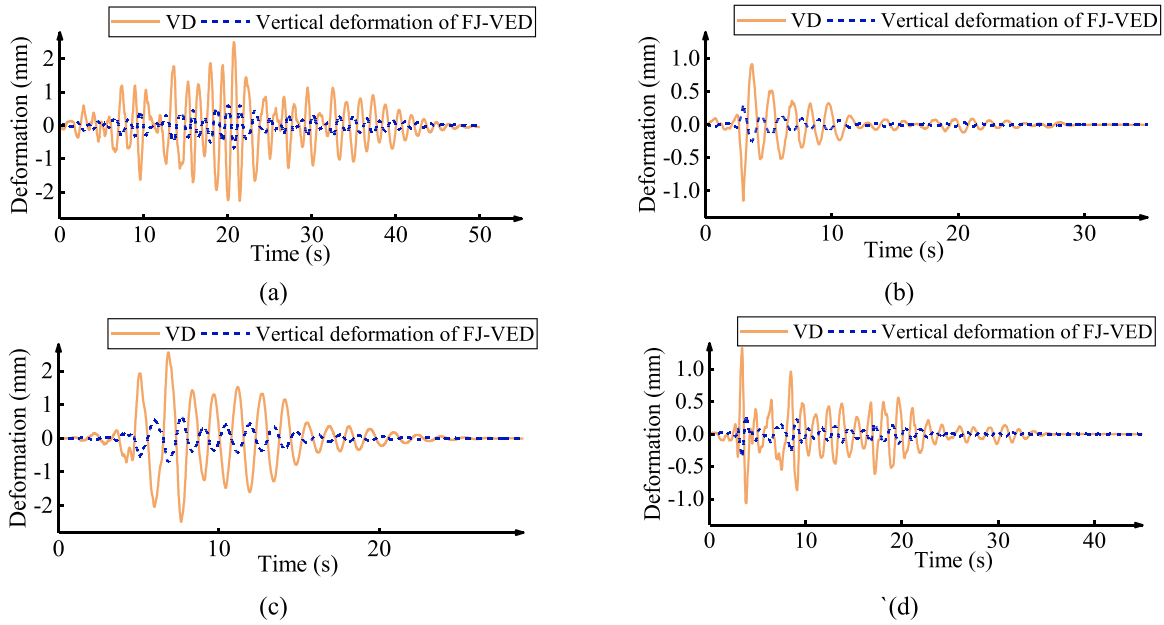


**Fig. 21.** Deformation time history curves of the viscous damper and vertical deformation of FJ-EVD on the 1st – 4th floor under the (a) artificial wave, (b) near-fault earthquake, (c) far-field earthquake, a(d) pulse earthquake.

$$\begin{cases} \text{maximize} \gamma_{\text{enhan}} \\ \text{subjectto} \begin{cases} \gamma_{\text{A}} \le \gamma_{\text{A,T}} \\ \gamma_{\theta} \le \gamma_{\theta,\text{T}} \end{cases} \end{cases} \tag{11}$$

where $\gamma_{\text{A,T}}$ and $\gamma_{\theta,\text{T}}$ are the preset target values of the maximum inter-story drift mitigation ratio and absolute acceleration mitigation ratio. To obtain the design parameters, the optimization process can be accomplished by using the optimal toolbox in the MATLAB [49], such as genetic algorithm, simulated annealing algorithm, particle swarm algorithm, etc. The initial values for the optimization process are suggested to set as minimum values closed to zero. Following the proposed design method, the vibration control demand-oriented design procedure is summarized in Fig. 16 for reference.

## 4. Illustrative design case

The seismic performance of the airport control tower can be enhanced by the designed FJ-EVD through the utilization of the proposed demand-oriented design method, as detailed in this section. The effectiveness of this enhancement can be demonstrated through various design cases using nonlinear time history analysis.

### 4.1. Earthquake records and designed FJ-EVDs

For the time history analysis of design case, an artificial wave is generated with wideband frequency components and three earthquake waves, including a near-fault earthquake, a far-field earthquake and a pulse-like earthquake, are selected from PEER ground motion database. The detailed information is expressed in Table 3 and the corresponding response spectra are shown in Fig. 17. The targeted vibration control

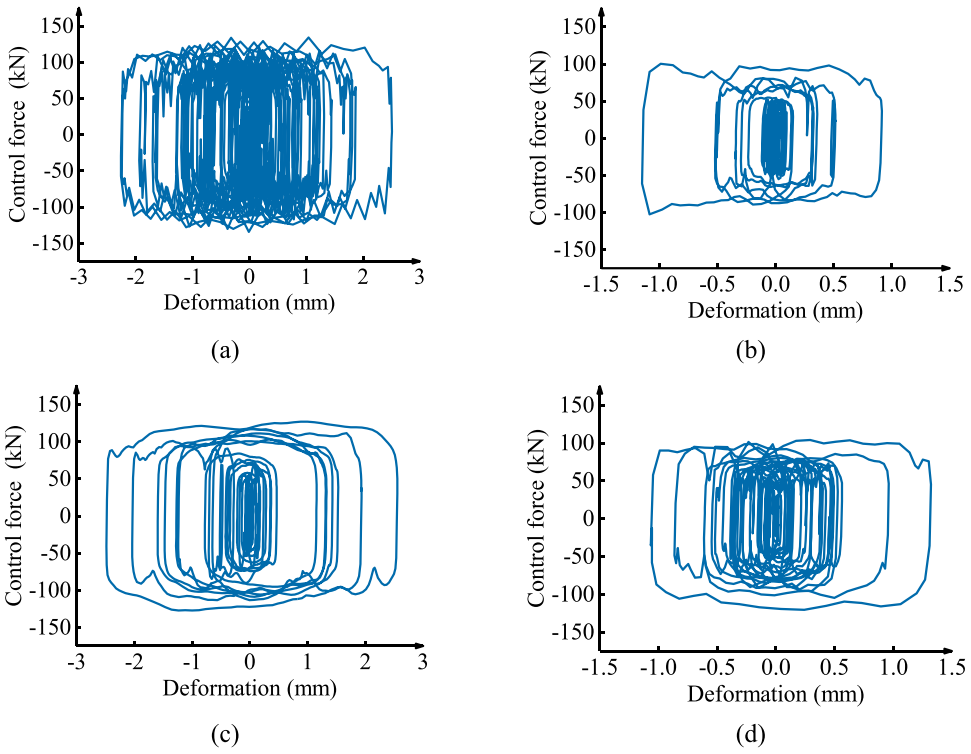


**Fig. 22.** Hysteretic curves of the viscous damper within the FJ-EVD on the 1st – 4th floor under the (a) artificial wave, (b) near-fault earthquake, (c) far-field earthquake, and (d) pulse earthquake.

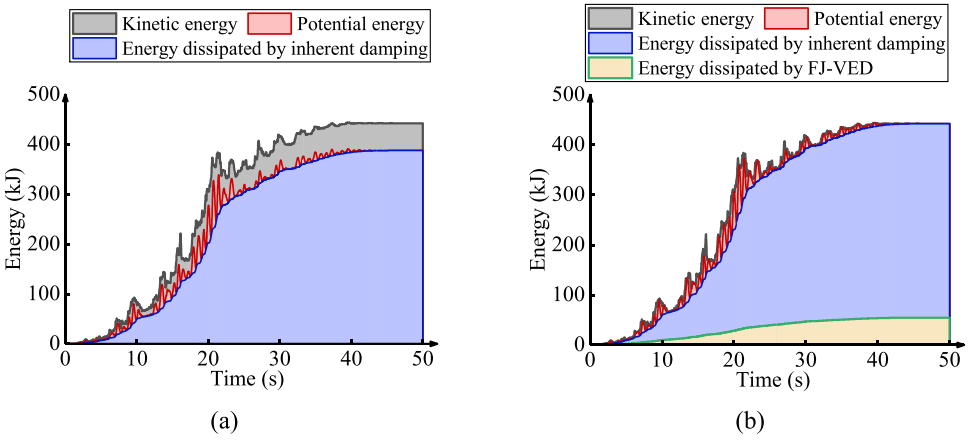


**Fig. 23.** Energy response curves of the (a) original structure and (b) FJ-VED-equipped airport control tower subjected to the artificial wave.

performance for all stories of the airport control tower is defined as $\gamma_0 = 0.70$ and $\gamma_A = 0.80$, achieving a 30 % reduction in the structural inter-story drift response and a 20 % reduction in the structural absolute acceleration response. Following the design procedure illustrated in the Section 3.4, the design parameters of the FJ-EVDs can be acquired by the 'fmincon' [50] toolbox, as indicated in Table 4.

### 4.2. Time history analysis results and discussions

The designed FJ-EVDs are attached to the airport control tower structure (ST1), enabling calculation of the maximum inter-story drift and absolute acceleration response. Seismic mitigation ratios are obtained by comparing these values to those of the original structure (ST0). To illustrate the damping enhancement effect of the FJ-EVD, the structure controlled by vertically installed VD with the same parameters as the FJ-EVD (ST2) is also analyzed and is shown in Table 5. It can be observed that the control efficiency of the FJ-EVD on the inter-story drift response is worse under W11, while that on the absolute acceleration response is worse under W10. However, the average values of the maximum inter-story drift mitigation ratio and absolute acceleration mitigation ratio are 0.65 and 0.79, respectively, which meet the requirements of the preset target. This result demonstrates the effectiveness of the proposed design procedure. In comparison with the FJ-EVD-equipped airport control tower (ST1), ST2 shows almost no effective utilization of the vertical deformation induced by floor rotation motions. Consequently, there is no damping enhancement effect, and the VD exhibits extremely small deformation, rendering it incapable of dissipating seismic energy. This observation necessitates the utilization of FJ-EVD for improved damping enhancement in the oscillation of high-rise structures within a bending model-based framework.

To illustrate the performance of the airport control tower structure controlled by FJ-EVDs, the inter-story drift and absolute acceleration

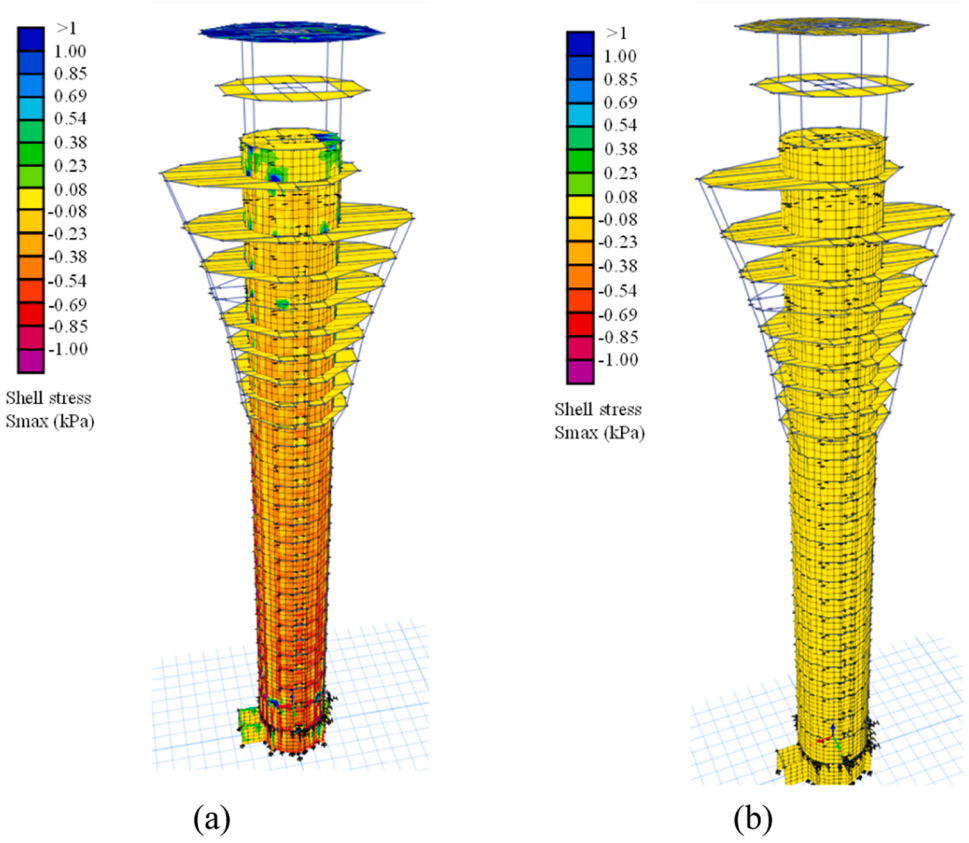


**Fig. 24.** Shell stress plots for the airport control tower (a) without FJ-EVD and (b) with FJ-EVD subjected to the artificial wave.

distributions along the structural height of the ST0, ST1 and ST2 are drawn in Fig. 18 and Fig. 19, whereas the inter-story drift and absolute acceleration time history curves of the 29$^{th}$ floor in the ST0, ST1 and ST2 are presented in Fig. 20. The time history curves for the deformation of VD and the vertical deformation of FJ-EVD are depicted in Fig. 21, demonstrating a notable enhancement in the deformation of VD. The corresponding hysteretic curves of the VD are shown in Fig. 22. The energy dissipation pattern is substantiated by the energy dissipation time history curves and shell stress plots of the original and controlled structures, shown in Fig. 23 and Fig. 24, respectively. It can be observed that, upon the installation of FJ-EVD, a greater amount of seismic energy is dissipated by VD within the FJ-EVD, resulting in a reduction in the seismic energy dissipated by the inherent structural damping. Consequently, the overall stress and damage experienced by the primary structure are significantly diminished.

## 5. Concluding remarks

This study proposes a novel frame jack-enhanced viscous damper (FJ-EVD) for the efficient seismic response mitigation in airport control towers by strategically employing frame jacks to augment viscous damping. A displacement amplification-oriented design formula is formulated with suggested nonlinear parameter sets of FJ-EVD. The key conclusions of this study can be summarized as follows:

(1) FJ-EVD yields a compact and highly efficient damping solution to the multiple seismic responses mitigation of the airport control tower in the bending-mode deformation process. In the design case, the displacement and absolute acceleration mitigation ratios of the structure with FJ-EVDs are $\gamma_\theta = 0.65$ and $\gamma_A = 0.79$, while that of the structure with conventional viscous dampers are $\gamma_\theta = 0.98$ and $\gamma_A = 0.97$, illustrating that the FJ-EVD demonstrates more significant mitigation effects for the structural acceleration and displacement than conventional viscous damper.

(2) The nonlinear viscous damper within the FJ-EVD is significantly and flexibly amplified due to the implemented jack frame and vertical installation approach, resulting in improved energy dissipation and vibration mitigation efficiency. The vertical deformation of the frame jack is amplified by a factor of 3 to 4 compared to the deformation of the viscous damper. Specifically, the recommended frame control angle and damping exponent coefficients for the FJ-EVD are provided to ensure the simultaneous control of crossing stories, making the system suitable for high-rise towers with limited installation space.

(3) Following the proposed displacement amplification-oriented design methodology, the FJ-EVD demonstrates superior effectiveness and robust control performance compared to conventional viscous dampers optimized under the same criterion. Additionally, the target displacement and acceleration control demands are met with optimized displacement amplification benefits. This study contributes to an enhanced damping solution and facilitated design parameters for bending deformation control of special air control towers through the implementation of the proposed FJ-EVD.

(4) Upon the deployment of FJ-EVD across diverse seismic scenarios, a notable enhancement in seismic energy dissipation is observed, primarily attributed to the nonlinear viscous dampers integrated within the FJ-EVD. This heightened dissipation is instigated by the activation of the bending-mode vibration process. Consequently, a substantial decrease in seismic energy dissipation attributed to the inherent structural damping mechanism is observed, leading to a marked reduction in overall stress levels and structural damage to the primary structures. Future research

will focus on conducting experimental tests using full-scale FJ-EVD installations and relevant airport control tower models, with consideration given to structural nonlinearity.

## CRediT authorship contribution statement

**Yijia Ma:** Writing – review & editing, Writing – original draft, Software, Validation. **Chao Luo:** Funding acquisition, Validation, Writing – review & editing. **Zhipeng Zhao:** Writing – review & editing, Writing – original draft, Visualization, Supervision, Investigation, Funding acquisition, Conceptualization. **Kai Yang:** Writing – review & editing, Writing – original draft, Validation, Software, Resources, Methodology, Investigation, Formal analysis. **Zhenhua Xu:** Writing – review & editing, Writing – original draft, Software, Resources, Investigation. **Minjun Wu:** Writing – review & editing, Writing – original draft, Software, Investigation.

## Declaration of Competing Interest

The authors declare that they have no known competing financial interests or personal relationships that could have appeared to influence the work reported in this paper.

## Acknowledgements

The authors thank the handling editor and anonymous reviewers for their time and effort in reviewing this paper. This study was supported by the Fundamental Research Funds for the Central Universities [Grant No. 22120240428], Hebei Provincial Natural Science Foundation of China [Grant No. E2024210049], and the Project of Central Guiding Local Science and Technology Development Funds (Fundamental Research Project) [Grant No. 216Z5402G]. The support is gratefully acknowledged.

## References

[1] Vafaei MA, Sophia C. Assessment of seismic design response factors of air traffic control towers. Bull Earthq Eng 2016;14(12):3441–61.
[2] Moravej H, Vafaei M. Seismic performance evaluation of an ATC tower through pushover analysis. Struct Eng Int 2019;29(1):144–9. https://doi.org/10.1080/10168664.2018.1468229.
[3] Hu XY, Zhao ZP, Yang K, Liao W, Chen QJ. Novel triple friction pendulum-tuned liquid damper for the wind-induced vibration control of airport control towers. Thin Walled Struct 2023;182:110337. https://doi.org/10.1016/j.tws.2022.110337.
[4] Moravej H, Vafaei M, Bakar SA. Seismic performance of a wall-frame air traffic control tower. Earthq Struct 2016;10(2):463–82.
[5] Wang JZ, Burton Henry V, Dai KS. Combination rules used to account for orthogonal seismic effects: state-of-the-art review. J Struct Eng 2019;145(11):03119001. https://doi.org/10.1061/(ASCE)ST.1943-541X.0002420.
[6] Wilcoski J, Heymsfield E. Performance and rehabilitation of type L FAA airport traffic control tower at San Carlos, California, for seismic loading. J Perform Constr Facil 2002;16(2):85–93. https://doi.org/10.1061/(asce)0887-3828(2002)16:2(85).
[7] Bozzoni F, Ozcebe AG, Balia A, Lai CC, Borzi B, Nascimbene R, et al. Seismic ground response analyses at an international airport in northern Italy by using a stochastic-based approach. J Theor Appl Mech 2020;58(2):499–511. https://doi.org/10.15632/jtam-pl/119017.
[8] Xu Y, Liu N, Hou X. Response analysis of a heat-absorbing tower under near-field earthquake. In: IOP conference series: Earth and environmental science. 1560. IOP Publishing Ltd.; 2020, 012039.
[9] Kiliç I, Bozdogan KB, Aydin S, Gök SG, Gündogan S. Determination of dynamic characteristics of tower type structures: the case of Kirklareli Hizirbey Mosque Minaret. J Polytech Politek Derg 2020;23(1):19–26. https://doi.org/10.2339/politeknik.481857.
[10] Zhao ZP, Wang YC, Hu XY, Weng DG. Seismic performance upgrading of containment structures using a negative-stiffness amplification system. Eng Struct 2022;262:114394. https://doi.org/10.1016/j.engstruct.2022.114394.
[11] Zhao ZP, Wang YC, Chen QJ, Qiang HF, Hong N. Enhanced seismic isolation and energy dissipation approach for the aboveground negative-stiffness-based isolated structure with an underground structure. Tunn Undergr Space Technol 2023;134:105019. https://doi.org/10.1016/j.tust.2023.105019.
[12] Zhao ZP, Tang YC, Hong N, Chen QJ, Du YF. Interaction-performance-driven design of negative-stiffness friction pendulum systems for aboveground structure–connected underground structure–soil system with ground motion effects. J Build Eng 2024;88:108970. https://doi.org/10.1016/j.jobe.2024.108970.
[13] Wang JZ, Liu K, Li A, Dai KS, Yin YX, Li JH. Shaking table test of a 1:10 scale thermal power plant building equipped with passive control systems. Eng Struct 2021;232:111804. https://doi.org/10.1016/j.engstruct.2020.111804.
[14] Wu MJ, Zhao ZP, Zhang RF, Zhang BB, Tang YC. Stability evaluation and design of negative stiffness amplifying damper-incorporated nonlinear structures. Eng Struct 2024;314:118241. https://doi.org/10.1016/j.engstruct.2024.118241.
[15] Zhao ZP, Chen QJ, Hu XY, Zhang RF. Enhanced energy dissipation benefit of negative stiffness amplifying dampers. Int J Mech Sci 2023;240:107934. https://doi.org/10.1016/j.ijmecsci.2022.107934.
[16] Zhu XY, Pan R, Li JB, Lin G. Study of isolation effectiveness of nuclear reactor building with three-dimensional seismic base isolation. Eng Comput 2022;39(4):1209–33. https://doi.org/10.1108/ec-11-2020-0637.
[17] Habieb AB, Valente M, Milani G. Effectiveness of different base isolation systems for seismic protection: numerical insights into an existing masonry bell tower. Soil Dyn Earthq Eng 2019;125:105752. https://doi.org/10.1016/j.soildyn.2019.105752.
[18] Atashfaraz B, Taiyari F, Raad HH, Formisano A. Post-tensioned tendons for enhancing the seismic behaviour of base-isolated monopole transmission towers. Eng Struct 2021;247:113222. https://doi.org/10.1016/j.engstruct.2021.113222.
[19] Liang SH, Zhang ZQ, Li AQ. Seismic reduction principle and response analysis of variable damping viscous damper system. Int J Struct Integr 2024;15(1):31–60. https://doi.org/10.1108/ijsi-08-2023-0085.
[20] Pratesi F, Sorace S, Terenzi G. Analysis and mitigation of seismic pounding of a slender R/C bell tower. Eng Struct 2014:7123–34. https://doi.org/10.1016/j.engstruct.2014.04.006.
[21] Wu QY, Dai JZ, Zhu HP. Optimum design of passive control devices for reducing the seismic response of twin-tower-connected structures. J Earthq Eng 2018;22(5):826–60. https://doi.org/10.1080/13632469.2016.1264332.
[22] Tang Z, Zhu HP, Luo H, Li T. Performance of a force-restricted viscous mass damper incorporated into base-isolated liquid storage tanks. Structures 2024;61:106002. https://doi.org/10.1016/j.istruc.2024.106002.
[23] Ijmulwar SS, Patro SK. Seismic design of reinforced concrete buildings equipped with viscous dampers using simplified performance-based approach. Structures 2024;61:106020. https://doi.org/10.1016/j.istruc.2024.106020.
[24] Luo HS, Du LZ, Zheng CF, Zhang SB, Bu XH, Wang TW. Seismic performance of graded energy dissipation damper for shield tunnel with variable mode. Soil Dyn Earthq Eng 2024;178:108516. https://doi.org/10.1016/j.soildyn.2024.108516.
[25] Zhao Z, Dai K, Lalond ER, Meng J, Li B, Ding Z, et al. Studies on application of scissor-jack braced viscous damper system in wind turbines under seismic and wind loads. Eng Struct 2019;196:109294.
[26] Gu JP, Qin YX, Xia YY, Jiao QQ, Gao HB, Zhang YY, et al. Research on dynamic characteristics of composite towering structure. Int J Appl Mech 2021;13(8):2150096. https://doi.org/10.1142/s1758825121500964.
[27] Dhorat A, Al-Obaidi MA, Mujtaba IM. Dynamic modelling and operational optimisation of natural draft cooling towers. Therm Sci Eng Prog 2019;9:930–43. https://doi.org/10.1016/j.tsep.2018.10.013.
[28] Chen X, Zhao L, Zhao SY, Ke ST, Cao SY, Ge YJ. Tornado-induced collapse analysis of a super-large reinforced concrete cooling tower. Eng Struct 2022;269:114834. https://doi.org/10.1016/j.engstruct.2022.114834.
[29] Lingaraju MKC, Girisha SK, Channabasappa SB, Karigowda M. A study on dynamic behavior of natural draft cooling tower considering the effect of soil-structure interaction. Civ Environ Eng Rep 2021;31(4):17–32. https://doi.org/10.2478/ceer-2021-0047.
[30] Castelli F, Grasso S, Lentini V, Sammito MSV. Effects of soil-foundation-interaction on the seismic response of a cooling tower by 3D-FEM analysis. Geosciences 2021;11(5):200. https://doi.org/10.3390/geosciences11050200.
[31] Zhao SQ, Lu Z, Fan QQ, Dai KS. Vibration control effect analysis of PTMD in wind turbine tower under multi-hazard action of earthquake and vortex-induced wind. Int J Struct Stab Dyn 2024:2550021. https://doi.org/10.1142/s021945542550021x.
[32] Wang LK, Zhou Y, Shi WX. Seismic multi-objective stochastic parameters optimization of multiple tuned mass damper system for a large podium twin towers structure. Soil Dyn Earthq Eng 2024;177. https://doi.org/10.1016/j.soildyn.2023.108428.
[33] Yao S, Liu C, Chen X, Tang BJ, Sun Y, Zhang ZQ. Hysteretic nonlinear SMA-TMD for wind-wave-induced vibration mitigation of monopile offshore wind turbines considering stiffness degradation. Ocean Eng 2024;294:116787. https://doi.org/10.1016/j.oceaneng.2024.116787.
[34] Liu KF, Liu YH, Chang CM, Tan P. Design and application of a novel eddy current damper for a high-rise sightseeing tower. Struct Eng Mech 2023;86(4):573–87. 10.12989/sem.2023.86.4.573.
[35] Cheng XS, Qi GJ, Guoliang L, Chen JC. TLD optimal vibration control for elevated concrete water towers. Eng Res Express 2024;6(1):015106. https://doi.org/10.1088/2631-8695/ad2d26.
[36] Shahrbabaki NE, Nekooei M, Hassanabad MG. A new method of using liquid damper to reduce the displacement of the monopile offshore platform against seismic loads. J Mar Sci Appl 2023;22(2):324–33. https://doi.org/10.1007/s11804-023-00325-x.
[37] Li YH, Li AQ, Deng Y. Performance investigation of circular TLD devices used in wind turbine generation tower via both experiment and numerical simulation. J Vib Eng Technol 2021;9(7):1715–32. https://doi.org/10.1007/s42417-021-00323-9.

[38] Konar T, Ghosh AD. Flow damping devices in tuned liquid damper for structural vibration control: a review. Arch Comput Methods Eng 2021;28(4):2195–207. https://doi.org/10.1007/s11831-020-09450-0.
[39] Lei Y, He MY, Lai ZL, Lin SZ. Identification of flexible buildings with bending deformation and the unmeasured earthquake ground motion. Sci China-Technol Sci 2015;58(3):454–61. https://doi.org/10.1007/s11431-014-5755-2.
[40] Wu J, Qi C, Zhang F, Lei Y, Zheng Z. State-input system identification of tall buildings under unknown seismic excitations based on modal Kalman filter with unknown input. J Aerosp Eng 2021;34(4):04021040.
[41] Aljwim K, Alih S, Vafaei M, Aisyah S. Seismic fragility curves for tall concrete wall building in Malaysia subjected to near-field earthquakes. International. J Eng Res Technol 2020:2205–12.
[42] Aisyah S, Vafaei M, Alih SC, Aljwim K. Seismic fragility of tall concrete wall structures in Malaysia under far-field earthquakes. Open Civ Eng J 2019;13. https://doi.org/10.2174/1874149501913010140.
[43] Zhou C, Tian M, Guo K. Seismic partitioned fragility analysis for high-rise RC chimney considering multidimensional ground motion. Struct Des Tall Spec Build 2019;28(1):e1568. https://doi.org/10.1002/tal.1568.
[44] Lyu Q, Zhang HQ, Fu B, Zhu BJ, Liu LK. Experimental study on the effect of nonlinear viscous dampers on base-isolated structures under near-fault earthquakes. Structures 2024;61:105995. https://doi.org/10.1016/j.istruc.2024.105995.
[45] Chopra AK, Naeim F. Dynamics of structures: Theory and applications to earthquake engineering. 4th Edition. Upper Saddle River, NJ: Prentice Hal; 2012.
[46] ETABS, Building analysis and design. In: Computers and Structures, Inc; 2021.
[47] Cole SW, Xu Y, Burton PW. Seismic hazard and risk in Shanghai and estimation of expected building damage. Soil Dyn Earthq Eng 2008;28(10):778–94. https://doi.org/10.1016/j.soildyn.2007.10.008.
[48] Goulet CA, Kishida T, Ancheta TD, Cramer CH, Darragh RB, Silva WJ, et al. PEER NGA-east database. Earthq Spectra 2021;37(1):1331–53.
[49] The MathWorks Inc, Optimization toolbox documentation. In: The MathWorks, Inc.; 2024.
[50] Byrd RH, Gilbert JC, Nocedal J. A trust region method based on interior point techniques for nonlinear programming. Math Program 2000;89(1):149–85. https://doi.org/10.1007/PL00011391.